

Impact of recent COMPASS data on polarized parton distributions and structure functions

M. Salimi-Amiri,^{*} A. Khorramian,[†] and H. Abdolmaleki[‡]
Faculty of Physics, Semnan University, 35131-19111, Semnan, Iran

F. I. Olness
Department of Physics, Southern Methodist University, Dallas, TX 75275-0175, USA[§]
 (Dated: December 14, 2024)

We perform a new extraction of polarized parton distribution functions (PPDFs) from the spin structure function experimental data in the fixed-flavor number scheme (FFNS). In this analysis, we include recent proton and deuteron spin structure functions obtained by the COMPASS collaboration. We examine the impact of the **new** COMPASS proton and deuteron data on the polarized parton densities and compare with results from our previous study (KATAO PPDFs) which used the Jacobi polynomial approach. We find the extracted PPDFs of the proton, neutron, and deuteron structure functions are in very good agreement with the experimental data. The results for extracted PPDFs are also compared with available theoretical models from the literature.

PACS numbers: 13.60.Hb, 12.39.-x, 14.65.Bt

CONTENTS

I. Introduction	2	4. COMPASS xg_1^N Structure Functions vs. x	9
II. Theoretical Formalism	2	5. $\alpha_s(Q^2)$ Comparisons	9
III. Input Parameterization and Data Sets	3	C. Moments and Sum Rules	10
A. Parameterization of the polarized parton densities	3	1. PPDF Moments	11
B. Overview of experimental data set	5	2. Structure Function Moments $\Gamma_1^N(Q^2)$	11
IV. Results of the QCD Analysis	6	3. Bjorken Sum Rule, $xg_1^{NS}(x, Q^2)$ and $\Gamma_1^{NS}(Q^2)$	11
A. Analysis Outline	7	4. $g_2^N(x, Q^2)$ Structure Functions	11
1. The fits: Base, Fit A, and Fit B	7	D. The Proton Spin	11
B. Structure Functions and PPDFs	7	V. Conclusions	14
1. The xg_1^N Structure Functions vs. Q^2	7	Acknowledgments	14
2. The Polarized PDFs (PPDFs)	7	References	14
3. Comparison of {Base, Fit A, Fit B} on PPDFs	8		

^{*} Maryam.salimi.amiri@semnan.ac.ir

[†] Khorramiana@semnan.ac.ir

[‡] Abdolmaleki@semnan.ac.ir

[§] olness@smu.edu

I. INTRODUCTION

One of the principal goals of Quantum Chromodynamics (QCD) has been the detailed investigation of the spin structure of the nucleon and nuclei, as well as the determination of the partonic composition of their spin projections. The extraction of polarized or spin-dependent parton distribution functions has been recognized as a longstanding issue of physical interest [1, 2], and theoretical studies on the spin structure of the nucleon have been discussed extensively in several reviews [3–7].

Determinations of polarized parton distribution functions (PPDFs) with an estimate of their uncertainties have been presented in multiple studies [8–40]. The variation among these PPDFs sets can be due to a number of factors including the choice of experimental data sets, the form of the parameterization and uncertainty calculation, as well as the details of the QCD analysis such as the treatment of heavy quarks or higher-twist corrections.

The results from various calculations can lead to a wide range of expectations for the polarized observables; hence, it is illuminating to compare the results of different methodologies to the experimental measurements. In our previous analysis, we performed the detailed pQCD analysis of PPDFs using the orthogonal Bernstein and Jacobi polynomial methods at next-to-leading-order (NLO) [41–43]. Other theoretical studies implementing a QCD analysis on the spin structure of the nucleon using orthogonal polynomials have been reported in Refs. [44–47]. Thus, one goal of our investigation is to revisit this topic using a Mellin moment approach instead of the orthogonal polynomial approach.

For the present study, we will focus on the polarized structure functions of the nucleon $g_1^{p,n,d}(x, Q^2)$ which play an important role in the behavior of polarized parton distribution functions (PPDFs). Polarized DIS lepton-nucleon scattering has been measured by DESY [48–50], SLAC [51–57], COMPASS[58–62], CLAS [63] and JLAB [64].

Recently, the COMPASS collaboration [65, 66] extracted new DIS measurements of the polarized proton and deuteron structure functions for the region of $0.0035 < x < 0.575$, $1.03 < Q^2 < 96.1 \text{ GeV}^2$ and $0.0045 < x < 0.569$, $1.03 < Q^2 < 74.1 \text{ GeV}^2$, respectively. Thus, we will combine the data sets used in Ref. [41] with the COMPASS16 and COMPASS17 data sets to extract improved polarized structure functions and PPDFs.

The plan of this paper is as follows. In Sec. II, we review the theoretical framework and basic formalism of the polarized structure function analysis based on the inverse Mellin technique. In Sec. III we outline the parameterization of PPDFs and the selection of the data sets. In Sec. IV, we present the structure functions, PPDFs, and moments obtained in our fit, and compare these both to our earlier KATAO fit (using orthogonal polynomials) as well as other results from the literature; this also includes an evaluation of the impact of the new COMPASS

data sets. Finally, in Sec. V, we provide a summary and concluding remarks.

II. THEORETICAL FORMALISM

The QCD formalism allows us to express the spin dependent nucleon structure function $g_1(x, Q^2)$ in terms of a Mellin convolution of the polarized non-singlet δq_i^{NS} , the polarized singlet $\delta\Sigma$, and the polarized gluon δg distributions with the corresponding Wilson coefficient functions δC_q^{NS} , δC_q^S and δC_g . The polarized structure function is then given by [4]

$$g_1(x, Q^2) = \frac{1}{2} \sum_{j=1}^{n_f} e_j^2 \left\{ \delta q_j^{NS} \otimes \left[1 + \frac{\alpha_s}{2\pi} \delta C_q^{NS} \right] \right. \\ \left. - \frac{1}{n_f} \delta\Sigma \otimes \left[1 + \frac{\alpha_s}{2\pi} \delta C_q^S \right] \right. \\ \left. + \frac{\alpha_s}{2\pi} \delta g(x, Q^2) \otimes \delta C_g \right\}, \quad (1)$$

where e_j denotes the charge of the j th quark flavor, N_f is the number of light flavors, x is the Bjorken variable, $Q^2 = -q^2$ is four-momentum transfer, and the symbol \otimes denotes the Mellin convolution. The coefficient functions δC_i which we use in the present analysis are calculated in the $\overline{\text{MS}}$ -scheme at the next-to-leading order [67–70]; in particular, we make use of the Pegasus routines [71]. The spin dependent flavor non-singlet distribution δq_j^{NS} evolve independently, while the spin dependent singlet $\delta\Sigma$ and gluon distributions δg are coupled in the QCD evolution.

In the above equation, the polarized non-singlet and singlet PPDFs are expressed by the individual spin dependent quark flavor contributions as

$$\delta\Sigma = \sum_{j=1}^{N_f} [\delta q_j + \delta \bar{q}_j], \quad (2)$$

$$\delta q_j^{NS} = \delta q_j + \delta \bar{q}_j - \frac{1}{N_f} \delta\Sigma, \quad (3)$$

where δq_j is the polarized quark distribution function of the j th light flavor.

In our fits, we will take the strong coupling constant $\alpha_s(Q_0^2)$ at initial scale Q_0^2 as a free parameter to be fit. The evolution of the strong coupling constant $\alpha_s(Q^2)$ can be obtained from the QCD renormalization group equation and is determined by the β -function, $\beta(Q^2)$:

$$\frac{d\alpha_s(Q^2)}{d \log(Q^2)} = \beta(Q^2) = -\beta_0 \alpha_s^2(Q^2) - \beta_1 \alpha_s^3(Q^2) + O(\alpha_s^4). \quad (4)$$

Here we have expanded the β -function in powers of α_s out to NLO, and the first two coefficients can be computed in the $\overline{\text{MS}}$ -scheme to be $\beta_0 = 11 - \frac{2}{3}N_f$ and $\beta_1 = 102 - \frac{38}{3}N_f$. Thus, given the value of $\alpha_s(Q_0^2)$ at the

initial scale Q_0^2 we can numerically solve the differential equation Eq.(4) for any Q^2 scale [71]. For the present analysis, we will work in the FFNS with $N_f = 3$ light partonic flavors $\{u, d, s\}$.

For our fit we will use the spin dependent proton, neutron, and deuteron structure functions. The spin dependent deuteron structure function $xg_1^d(x, Q^2)$ can be represented in terms of the proton and neutron structure functions, $xg_1^p(x, Q^2)$ and $xg_1^n(x, Q^2)$ using the relation

$$xg_1^d(x, Q^2) = \frac{1}{2} \left(1 - \frac{3}{2}\omega_D \right) [xg_1^p(x, Q^2) + xg_1^n(x, Q^2)] ,$$

where $\omega_D = 0.05 \pm 0.01$ is the D -state wave probability for the deuteron [72].

For comparison with the data, we will need to compute the PPDFs and structure functions at a variety of Q^2 scales. The evolution in Q^2 is performed using the well-known DGLAP collection of integro-differential evolution equations [73, 74] which can be solved analytically after a conversion from x -space to Mellin N -moment space.

The N 'th Mellin moments of the spin dependent parton densities $\delta f(x)$ are defined to be

$$\delta f(N) = \int_0^1 x^{N-1} \delta f(x) dx . \quad (5)$$

The Mellin transform will decompose the convolution of parton densities $\delta f(x)$ of Eq. (1) into a product of Mellin moments:

$$[f \otimes g](N) \equiv \int_0^1 dx^{n-1} \int_z^1 \frac{dy}{y} f\left(\frac{x}{y}\right) g(y) = f(N)g(N) .$$

To invert the Mellin transform, the argument N is analytically continued to the complex plane. Note that the basic method of solving the spin dependent non-singlet, singlet, and gluon evolution equations in Mellin space is reported in the literature in detail [68, 69, 75, 76].

The solution of the flavor non-singlet, singlet and gluon evolution equations at NLO are given by

$$\begin{aligned} \delta q_j^{\text{NS}}(N, Q^2) &= \left(\frac{a_s}{a_0} \right)^{-P_{\text{NS}}^{(0)}/\beta_0} \times \\ &\left[1 - \frac{1}{\beta_0} (a_s - a_0) \left(\delta P_{\text{NS}}^{(1)} - \frac{\beta_1}{\beta_0} P_{\text{NS}}^{(0)} \right) \right] \delta q_j^{\text{NS}}(N, Q_0^2) , \end{aligned} \quad (6)$$

$$\begin{aligned} \left(\frac{\delta \Sigma(N, Q^2)}{\delta g(N, Q^2)} \right) &= [1 + a_s U_1(N)] L(N, a_s, a_0) [1 - a_0 U_1(N)] \\ &\times \left(\frac{\delta \Sigma(N, Q_0^2)}{\delta g(N, Q_0^2)} \right) , \end{aligned} \quad (7)$$

where $a_s \equiv a_s(Q^2)$, $a_0 = a_s(Q_0^2)/4\pi$, $\delta P_{\text{NS}}^{(0)}$ and $\delta P_{\text{NS}}^{(1)}$ denote the LO and NLO non-singlet splitting functions.

Given the initial PPDFs at input scale Q_0^2 , equations (6) and (7) yield the distributions $\delta q^{\text{NS}}(N, Q^2)$,

$\delta \Sigma(N, Q^2)$ and $\delta g(N, Q^2)$ in Mellin N -space for any scale. We can then transform back to x -space to obtain $\delta f(x)$ by performing a contour integral in the complex plane [77]:

$$\delta f(x) = \frac{1}{\pi} \int_0^\infty dz \operatorname{Im} \left[\exp(i\phi) x^{-c(z)} \delta f[c(z)] \right] , \quad (8)$$

where we choose $c(z) = 1.1 + \rho[\cos(3\pi/4) + i \sin(3\pi/4)]$. The basic framework of this method is described in the literature [24, 32, 77]. The resulting $\delta f(x)$ for all PPDFs depends on the initial value of $\alpha_s(Q_0^2)$ and unknown parameters of the spin dependent parton distributions; we will now discuss our parameterization form.

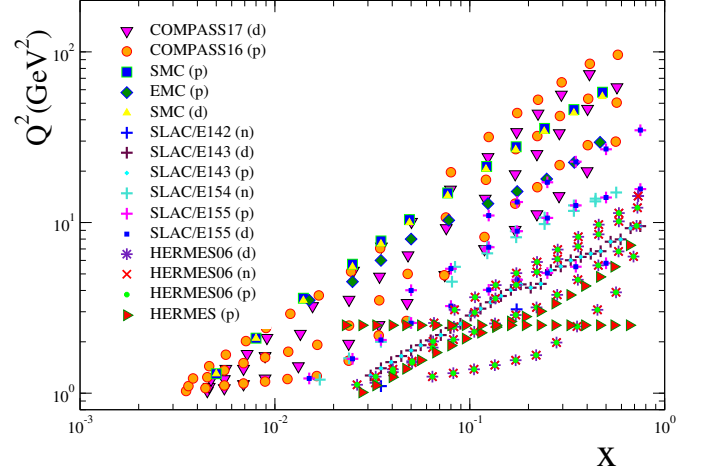


Figure 1. Experimental data sets used in our fit of proton, deuteron and neutron structure functions in the $\{x, Q^2\}$ plane.

III. INPUT PARAMETERIZATION AND DATA SETS

To study the impact of the recent COMPASS16 [65] and COMPASS17 [66] data on the spin dependent parton distribution functions, we will start by comparing to our previous KATAO [41] results; hence, our initial parameterization and χ^2 minimization will be based on this work.

A. Parameterization of the polarized parton densities

For the parameterization of the spin dependent parton densities in x space at our initial scale $Q_0^2 = 4 \text{ GeV}^2$,

$$x\delta q_j(x, Q_0^2) = \eta_j \mathcal{A}_j x^{\alpha_j} (1-x)^{\beta_j} (1+\gamma_j x) . \quad (9)$$

The free parameters are $\{\eta_j, \alpha_j, \beta_j, \gamma_j\}$, and we use the common notation $\delta q_j = \{\delta u_v, \delta d_v, \delta \bar{q}, \delta g\}$ for the partonic flavors up-valence, down-valence, sea, and gluon. In this functional form, the terms x^{α_j} and $(1-x)^{\beta_j}$ control

Experiment	Reference	Data	x -Range	Q^2 -Range	\mathcal{A}_i
		Type # data points	(GeV ²)		
HERMES	[49, 50]	g_1^p 39	0.028-0.66	1.01-7.36	1.000
HERMES06	[48]	g_1^p 51	0.026-0.731	1.12-14.29	0.999
SLAC/E143	[54]	g_1^p 28	0.031-0.749	1.27-9.52	1.000
SLAC/E155	[57]	g_1^p 24	0.015-0.750	1.22-34.72	1.024
SMC	[59]	g_1^p 12	0.005-0.480	1.30-58.0	1.000
EMC	[58]	g_1^p 10	0.015-0.466	3.50-29.5	1.011
COMPASS10	[60]	g_1^p 15	0.005-0.568	1.10-62.10	0.994
COMPASS16	[65]	g_1^p 51	0.0035-0.575	1.03-96.1	1.000
Proton		230			
HERMES06	[48]	g_1^d 51	0.026-0.731	1.12-14.29	0.997
SLAC/E143	[54]	g_1^d 28	0.031-0.749	1.27-9.52	0.998
SLAC/E155	[55, 56]	g_1^d 24	0.015-0.750	1.22-34.79	0.999
SMC	[59]	g_1^d 12	0.005-0.479	1.30-54.80	0.999
COMPASS05	[61]	g_1^d 12	0.0051-0.4740	1.18-47.5	0.998
COMPASS06	[62]	g_1^d 15	0.0046-0.566	1.10-55.3	0.993
COMPASS17	[66]	g_1^d 43	0.0045-0.569	1.03-74.1	1.001
Deuteron		185			
HERMES	[49, 50]	g_1^n 9	0.033-0.464	1.22-5.25	0.999
HERMES06	[48]	g_1^n 51	0.026-0.731	1.12-14.29	1.000
SLAC/E142	[51]	g_1^n 8	0.035-0.466	1.10-5.50	0.999
SLAC/E154	[53]	g_1^n 17	0.017-0.564	1.20-15.00	0.999
Neutron		85			
<i>Total</i>		500			

Table I. Data sets for polarized DIS structure functions used in our QCD analysis inclusively covering $0.0035 \leq x \leq 0.75$ and $1 \leq Q^2 \leq 96.1$ GeV². For each experiment we provide the x and Q^2 ranges, the number of data points, and the fitted normalization shifts \mathcal{A}_i .

the low and large x behavior of the parton densities, respectively. The $(1 + \gamma_j x)$ factor controls the intermediate x . The maximal number of parameters which should be fitted for each flavor component is four $\{\eta_j, \alpha_j, \beta_j, \gamma_j\}$, and there are four flavor components $\{\delta u_v, \delta d_v, \delta \bar{q}, \delta g\}$; this yields a total of 16 degrees of freedom, but we will introduce some constraints to reduce the number of free parameters in order to achieve a stable and reliable minimum.

The \mathcal{A}_j and η_j parameters are not independent. Since the first moment of polarized parton densities plays an important role, the normalization constants \mathcal{A}_j are selected such that η_j are the first moments of spin dependent of parton densities $\delta q_j(x, Q_0^2)$; specifically $\eta_j = \int_0^1 dx \delta q_j(x, Q_0^2)$. Thus, the normalization factors \mathcal{A}_j can be computed to be:

$$\frac{1}{\mathcal{A}_j} = \left(1 + \gamma_j \frac{\alpha_j}{\alpha_j + \beta_j + 1}\right) \mathcal{B}(\alpha_j, \beta_j + 1) , \quad (10)$$

where $\mathcal{B}(m, n)$ is the Euler beta function.

We will presume a $SU(3)$ flavor symmetry such that $\delta \bar{q} \equiv \delta \bar{u} = \delta \bar{d} = \delta s = \delta \bar{s}$. As we mentioned before, by including only inclusive DIS data in the QCD fit, it is not possible to separate polarized quarks from polarized

anti-quarks. In fact, inclusive polarized DIS data constrain the total polarized quarks and anti-quarks combinations.¹

Using the above results, we can analytically compute the Mellin- N space transform of the polarized parton densities at the input scale of Q_0^2 :

$$\begin{aligned} \delta q_j(N, Q_0^2) &= \int_0^1 x^{N-1} \delta q_j(x, Q_0^2) dx \\ &= \eta_j \mathcal{A}_j \left(1 + \gamma_j \frac{N-1 + \alpha_j}{N + \alpha_j + \beta_j}\right) \\ &\quad \times \mathcal{B}(N-1 + \alpha_j, \beta_j + 1) . \end{aligned} \quad (11)$$

The first moments of the polarized valence distribution, δu_v and δd_v , can be fixed by utilizing the parameters F and D as measured in neutron and hyperon β -decays [78]. In fact q_3 and q_8 are the non-singlet combinations of the polarized parton densities:

$$\delta q_3 = (\delta u + \delta \bar{u}) - (\delta d + \delta \bar{d}) , \quad (12)$$

¹ In Ref. [77], we reported the results of QCD analysis using polarized DIS and the semi-inclusive DIS (SIDIS) asymmetry world data, and we extracted the PPDFs considering a light sea-quark decomposition.

	KATAO (Jacobi Poly.)	Base	Fit A	Fit B
η_{u_v}	0.928 (<i>fixed</i>)	0.928 (<i>fixed</i>)	0.928 (<i>fixed</i>)	0.928 (<i>fixed</i>)
α_{u_v}	0.535 ± 0.022	0.559 ± 0.019	0.552 ± 0.018	0.551 ± 0.017
β_{u_v}	3.222 ± 0.085	3.202 ± 0.080	3.192 ± 0.077	3.191 ± 0.075
γ_{u_v}	8.180 (<i>fixed</i>)	7.115 (<i>fixed</i>)	7.115 (<i>fixed</i>)	7.115 (<i>fixed</i>)
η_{d_v}	-0.342 (<i>fixed</i>)	-0.342 (<i>fixed</i>)	-0.342 (<i>fixed</i>)	-0.342 (<i>fixed</i>)
α_{d_v}	0.530 ± 0.067	0.652 ± 0.062	0.677 ± 0.060	0.681 ± 0.056
β_{d_v}	3.878 ± 0.451	3.742 ± 0.416	3.905 ± 0.413	3.892 ± 0.395
γ_{d_v}	4.789 (<i>fixed</i>)	2.125 (<i>fixed</i>)	2.125 (<i>fixed</i>)	2.125 (<i>fixed</i>)
$\eta_{\bar{q}}$	-0.054 ± 0.029	-0.285 ± 0.015	-0.292 ± 0.017	-0.291 ± 0.015
$\alpha_{\bar{q}}$	0.474 ± 0.121	0.562 ± 0.100	0.492 ± 0.090	0.493 ± 0.078
$\beta_{\bar{q}}$	9.310 (<i>fixed</i>)	12.384 (<i>fixed</i>)	12.384 (<i>fixed</i>)	12.384 (<i>fixed</i>)
$\gamma_{\bar{q}}$	0	0	0	0
η_g	0.224 ± 0.118	0.218 ± 0.087	0.167 ± 0.081	0.162 ± 0.074
α_g	2.833 ± 0.528	3.349 ± 0.438	3.220 ± 0.538	3.198 ± 0.520
β_g	5.747 (<i>fixed</i>)	7.645 (<i>fixed</i>)	7.645 (<i>fixed</i>)	7.645 (<i>fixed</i>)
γ_g	0	0	0	0
$\alpha_s(Q_0^2)$	0.381 ± 0.017	0.393 ± 0.014	0.396 ± 0.013	0.395 ± 0.013
$\chi^2_{\text{COMPASS16}}$	—	—	33.488	33.495
$\chi^2_{\text{COMPASS17}}$	—	—	—	27.195
χ^2	273.6	293.5	327.6	354.9
<i>dof</i>	370	397	448	491
χ^2/dof	0.74	0.74	0.73	0.72

Table II. Comparison of the parameter values and their statistical errors at the input scale $Q_0^2 = 4 \text{ GeV}^2$ in the different cases: KATAO (Jacobi polynomial method) [41], Base (without COMPASS16 and COMPASS17), Fit A (with COMPASS16), Fit B (with COMPASS16 and COMPASS17) obtained from the best fit to the data.

$$\delta q_8 = (\delta u + \delta \bar{u}) + (\delta d + \delta \bar{d}) - 2(\delta s + \delta \bar{s}) . \quad (13)$$

The first moments of the above distributions are found to be:

$$\int_0^1 dx \delta q_3 = \eta_{u_v} - \eta_{d_v} = F + D , \quad (14)$$

$$\int_0^1 dx \delta q_8 = \eta_{u_v} + \eta_{d_v} = 3F - D . \quad (15)$$

Using $F=0.464 \pm 0.008$ and $D=0.806 \pm 0.008$ from the literature [25], we find the first moments of δu_v and δd_v to be $\eta_{u_v} = +0.928 \pm 0.014$ and $\eta_{d_v} = -0.342 \pm 0.018$; in our QCD fit we will fix $\{\eta_{u_v}, \eta_{d_v}\}$ to these central values. The first moments of $\delta \bar{q}$ and δg do not have prior constraints, and these will be determined in the fit by the free parameters $\eta_{\bar{q}}$ and η_g .

The factor of $(1 + \gamma_j x)$ in Eq. (9) provides flexibility of the parameterization in the intermediate x region. This flexibility is beneficial for fitting the the polarized valence distributions $\delta u_v, \delta d_v$. In contrast, we find that the parameters $\gamma_{\bar{q}}$ and γ_g have a very mild impact on the fit and it is sufficient to set them to zero and remove these degrees of freedom. (We note the QCD analysis of polarized SIDIS data [77] is sensitive to the $\gamma_{\bar{q}}$ and γ_g parameters.)

We have now reduced the number of free parameters from 16 to 12. Preliminary fits indicate that some of

the parameters such as $\{\gamma_{u_v}, \gamma_{d_v}, \beta_{\bar{q}}, \gamma_g\}$ are very weakly constrained by the present data set; therefore we will also fix the values of these parameters, and we now have a remaining 8 free parameters for the PPDFs in addition to the QCD coupling constant $\alpha_s(Q_0^2)$ to fit from the data.

B. Overview of experimental data set

The notable advances of the experimental data of the inclusive polarized deep inelastic scattering on nucleons in recent years allows us to perform an improved QCD analysis of polarized structure functions in order to discern the spin-dependent partonic structure of the nucleon. For our analysis, we will include spin structure function data on protons from HERMES [48–50], E143 [54], E155 [57], SMC [59], EMC [58], and COMPASS [60, 65], and on deuterons from HERMES [48], E143 [54], E155 [55, 56], SMC [59] and COMPASS [61, 62, 66], and on neutrons from HERMES [48–50], E142 [51] and E154 [53]. This data set includes the recent proton data from COMPASS16 [65] (51 points), and the recent deuteron data from COMPASS17 [66] (43 points). This gives us a total of 500 experimental data points spanning a kinematic range of $0.0035 < x < 0.75$ and $1 < Q^2 < 96.1 \text{ GeV}^2$; these

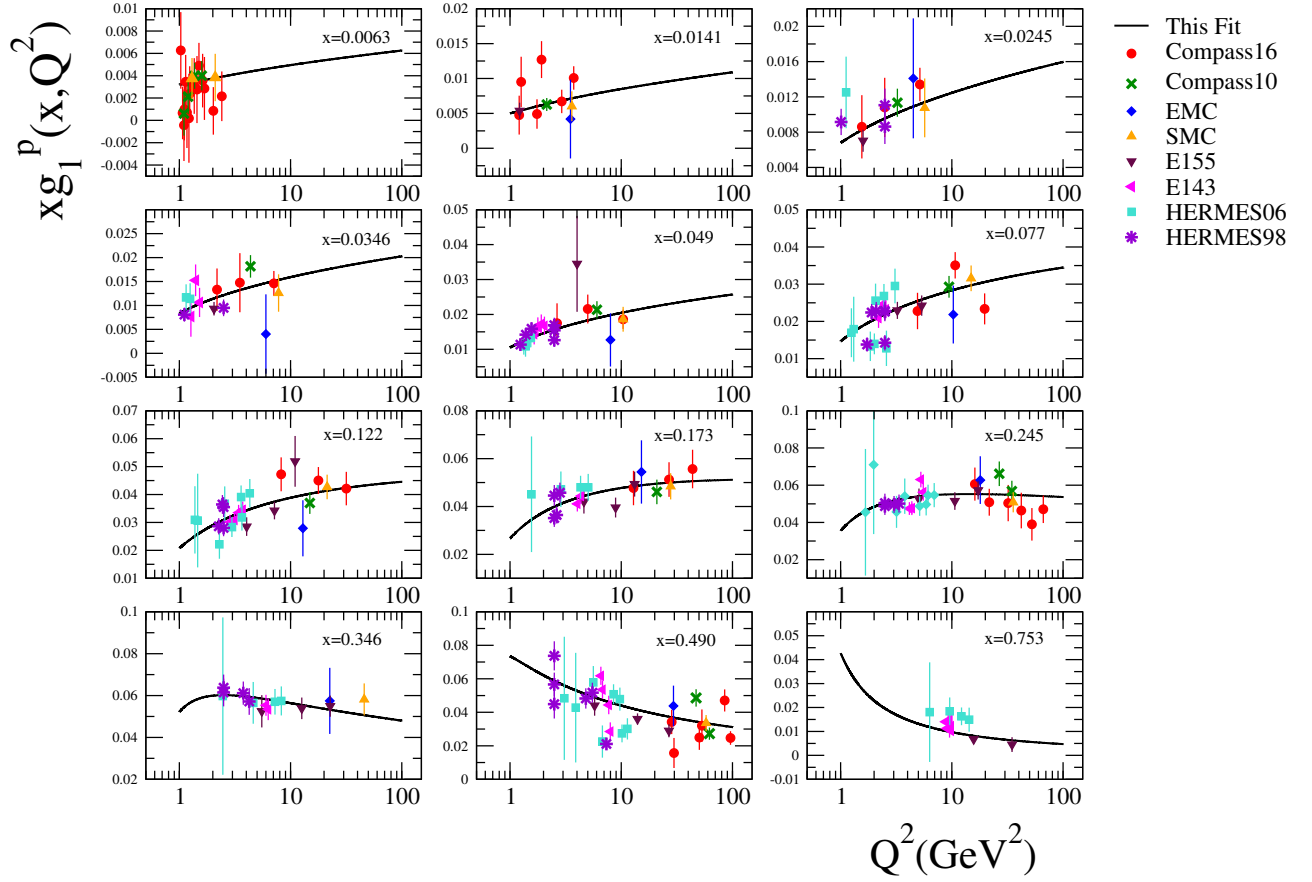


Figure 2. Polarized proton structure function $xg_1^p(x, Q^2)$ as function of Q^2 in intervals of x in comparison to experimental data of COMPASS16 [65], COMPASS10 [60], EMC [58], SMC [59], E155 [57], E143 [54], HERMES06 [48], HERMES98 [49, 50].

are displayed in Fig. 1, and the detailed information and references are summarized in Table I.

In this analysis we will evolve the PPDFs from the initial scale $Q_0^2 = 4 \text{ GeV}^2$ up to arbitrary scales to compare our theoretical predictions with the data across the full kinematic range. We construct a global χ^2 function using the experimental measurements g_1^{Exp} , the experimental uncertainty (statistical and systematic added in quadrature) Δg_1^{Exp} , and theoretical prediction g_1^{Theory} . Our χ^2 is constructed as follows:

$$\begin{aligned} \chi_{\text{global}}^2 &= \sum_{i=1}^{n^{Exp}} w_i \chi_i^2 \\ &= \sum_{i=1}^{n^{Exp}} w_i \left[\frac{(\mathcal{A}_i - 1)^2}{(\Delta \mathcal{A}_i)^2} + \sum_{j=1}^{n^{Data}} \left(\frac{\mathcal{A}_i g_{1,j}^{Exp} - g_{1,j}^{Theory}}{\mathcal{A}_i \Delta g_{1,j}^{Exp}} \right)^2 \right], \end{aligned} \quad (16)$$

where the i -index sums over all experimental data sets, and in each experimental data set the j -index sums over all data points. We introduce a weight w_i which allows us to apply separate weights to different experimental data sets; for the present analysis we choose all weights to be unity, $w_i = 1$.

These data sets include statistical and systematic errors which we combine in quadrature. There is also a normalization for each experiment \mathcal{A}_i and an associated uncertainty $\Delta \mathcal{A}_i$. The normalization shifts \mathcal{A}_i are fitted at the start of our procedure, and then fixed. We present these values in Table I, and find all the \mathcal{A}_i shifts are less than 1% except for a single value; for the SLAC/E155 experiment we find $\mathcal{A}_i = 1.024$.

As outlined in Sec. III A, we have a total of 9 unknown free parameters: 8 parameters describing the PPDFs at Q_0^2 , and also $\alpha_s(Q_0^2)$ as another free parameter. We will use the CERN library MINUIT package [79] to minimize χ^2 by varying the free parameters and obtain a best fit. We are now ready to extract the polarized parton densities.

IV. RESULTS OF THE QCD ANALYSIS

In this section, we will demonstrate how inclusion of the new COMPASS proton g_1^p data [65] and deuteron g_1^d data [66] influence our PPDFs.

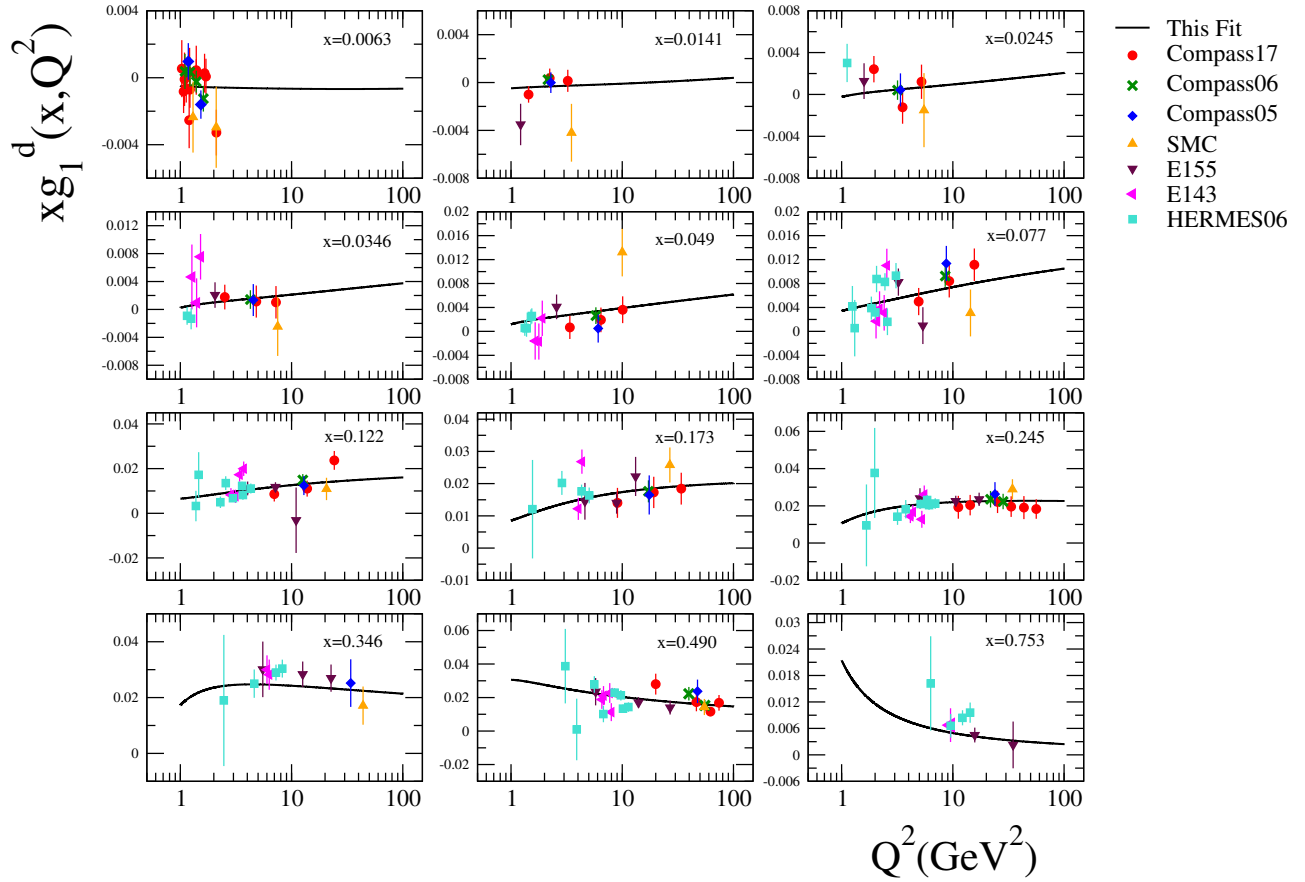


Figure 3. Polarized deuteron structure function $xg_1^d(x, Q^2)$ as function of Q^2 in intervals of x in comparison to experimental data of COMPASS17 [66], COMPASS06 [62], COMPASS05 [61], SMC [59], E155 [55, 56], E143 [54], HERMES06 [48].

A. Analysis Outline

1. The fits: Base, Fit A, and Fit B

We will divide our analysis into three steps. As a first step, we perform a fit with all the data of Table I with the *exception* of the COMPASS16 [65] and COMPASS17 [66] experimental data; this totals 406 data points, and we identify this as our “Base” fit. We then include the COMPASS16 proton data, and this is our “Fit A” which contains 457 data. Finally, we include the COMPASS17 deuteron data, and this is our “Fit B” with the full 500 data points. As Fit B contains the complete data set, we will use this for comparisons in Figs. 2, 3, 4, and 5 where it is identified as “This Fit.”

In Table II, the final values of the fit parameters for the different data sets are summarized. We find χ^2/dof is less than unity in all cases indicating a good quality of fit. Additionally, our fits compare well with our previous KATAO analysis where we find $\chi^2/dof=273.6/370$.

B. Structure Functions and PPDFs

1. The xg_1^N Structure Functions vs. Q^2

We will begin with the comparison of the xg_1^N structure functions as this is the primary input to our fit. In Figs. 2, 3, and 4, we display the comparison of our theoretical predictions with the structure function data for xg_1^p , xg_1^d and xg_1^n , respectively. The figures are given as a function of Q^2 at different values of x and are compared to all of the experimental data that we used in the present analysis. The theoretical predictions are in good agreement with the experimental measurements across the full x -range. In the following sections, we will investigate the impact of the new COMPASS measurements on the central values of the PPDFs and their uncertainties.

2. The Polarized PDFs (PPDFs)

Next we turn to the PPDFs themselves. Figure 5 displays the extracted $x\delta u_v(x)$, $x\delta d_v(x)$, $x\delta\bar{q}(x)$, and $x\delta g(x)$ PPDFs and with their associated uncertainties as compared with various other determinations from the litera-

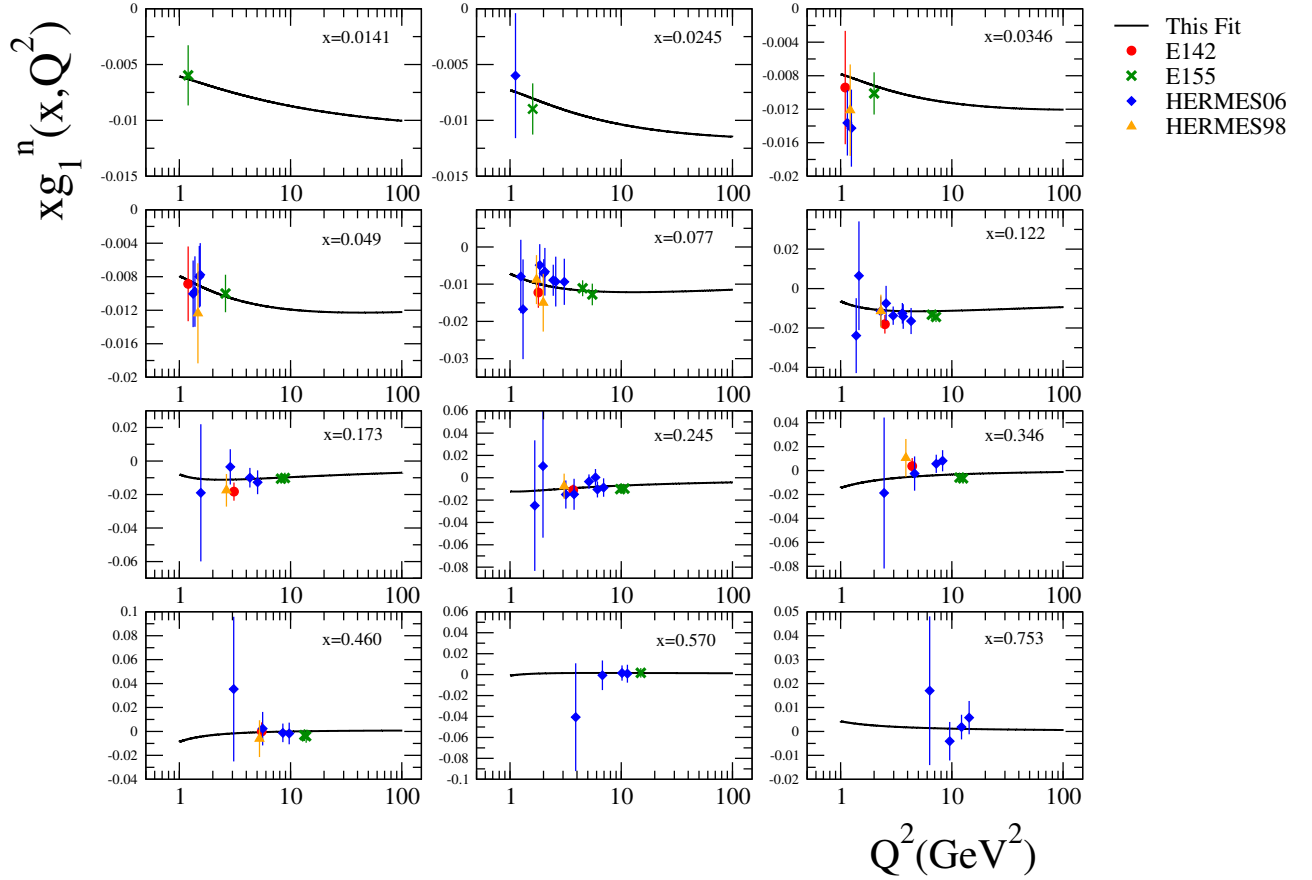


Figure 4. Polarized neutron structure function $xg_1^n(x, Q^2)$ as function of Q^2 in intervals of x in comparison to experimental data of E142 [51], E154 [53], HERMES06 [48], HERMES98 [49, 50].

ture [21, 25, 30, 32, 34, 41]. We derive the uncertainties of the polarized parton distributions for the different polarized observables using the covariance matrix elements of the QCD fit.

Examining Fig. 5 we find the spread of results for the $x\delta u_v$ distribution is comparatively narrow indicating this flavor component is well constrained. The results of “Fit B” are comparable to our previous analysis using the Jacobi polynomial expansion method (KATAO) [41], as well as many of the other results from the literature. Our results are slightly larger than DSSV and LSS in the small x region ($x \sim 0.01$) and BB in the larger x region ($x \sim 0.2$).

The $x\delta d_v$ distribution is also comparatively narrow suggesting this too is well constrained. Again, our results of “Fit B” are generally comparable to the other results from the literature, with “Fit B” yielding a slightly larger $x\delta d_v$ than DSSV and BB in the region $x \sim 0.1$.

For the $x\delta\bar{q}(x)$ distributions, we find a broader spread of both our results (“Fit B” and KATAO) and the other fits from the literature suggesting this component is less constrained. Specifically, “Fit B” roughly coincides with many of the other predictions, but the DSSV yields a smaller result and LSS yields a larger result.

Of all the components we examine, clearly the gluon

distribution $x\delta g$ has the widest spread of predictions and the greatest uncertainty. “Fit B” is similar to the KATAO results, but yields a smaller result in the region $x \sim 0.3$; compared to the other curves, these results generally give a smaller $x\delta g$ than the other predictions. In particular, in the region $x \sim 0.1$ AAC give the largest result and DSSV gives a negative results. Clearly, the $x\delta g$ distribution leaves much room for improvement and it will be interesting to see which predictions are favored by future data sets. Presumably, the choice of data sets (such as SIDIS) may contribute to these differences.

3. Comparison of {Base, Fit A, Fit B} on PPDFs

Since it is the new COMPASS data on xg_1^p and xg_1^d that represent the important new additions to our data set, we want to focus on the variations among our fits: {Base, Fit A, Fit B}.

To investigate the specific impact of COMPASS16 and COMPASS17 data sets, we compare our results for our individual fits: “Base” (without including COMPASS16 and COMPASS17), “Fit A” (including COMPASS16) and “Fit B” (including COMPASS16 and COMPASS17). These results are shown in Fig. 6 where we have displayed both the abso-

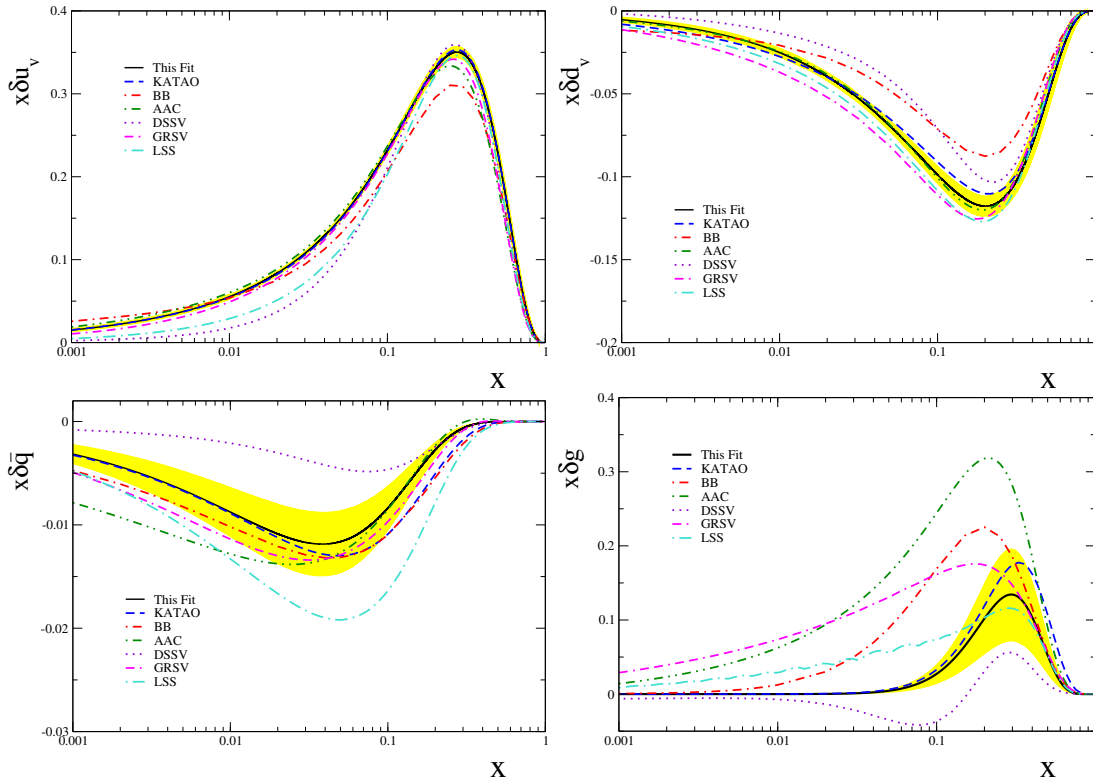


Figure 5. Our results for NLO polarized parton distributions at $Q_0^2 = 4 \text{ GeV}^2$. The corresponding PPDFs (the solid lines) with error bands compared to results obtained by KATAO [41], BB [32], AAC [25], DSSV [30], GRSV [21] and LSS [34]. For clarity, we only present our Fit B results, labeled hereas “This Fit.”

lute value of the PPDFs and also the ratio compared to our base fit.

As suggested by the results of Fig. 5, in Fig. 6 we find that $x\delta u_v(x)$ and $x\delta d_v(x)$ appear to be strongly constrained with little variation among the separate fits. Specifically, the variation is on the order of a percent except for the region at large x where the PPDFs vanish and they are no data constraints.

In contrast, $x\delta\bar{q}(x)$ and $x\delta g(x)$ do display some differences amount the fits due to the addition of the COMPASS data; the variations of “Fit A” and “Fit B” of Fig. 6 are quite similar, and these differ from the “Base” fit. The $x\delta\bar{q}(x)$ function displays some variation in the small x region $\lesssim 10^{-1}$ while the variation of $x\delta g(x)$ function is generally at larger $x \gtrsim 10^{-1}$; again, the very large x region should be discounted as before.

4. COMPASS xg_1^N Structure Functions vs. x

To examine how the fits change with the inclusion of the COMPASS data, we examine the partial χ^2 contributions to COMPASS16 and COMPASS17 data set for each of our fits: {Base, Fit A, Fit B}. If we compute χ^2 for the COMPASS16 data set using the “Base” fit (which does not include this data), we find a total χ^2 value of 34.67 for the 51 COMPASS16 data points, and when we

include this data in the fit (“Fit A”) it improves slightly to 33.48. Correspondingly, if we fit the COMPASS17 data set using the “Fit A” (which does not include this data), we find a total χ^2 value of 27.43 for the 43 COMPASS17 data points, and in the fit (“Fit B”) this is quite similar at 27.22. Thus, both the COMPASS16 and COMPASS17 data set are in reasonable agreement to the initial “Base” fit. The changes among the {Base, Fit A, Fit B} sets is most evident in the ratio plots of Fig. 6.

Finally, in Figs. 7 and 8, we directly compare our “Fit B” with the proton and deuteron polarized structure functions from COMPASS16 [65] and COMPASS17 [66] experimental data in a composite plot; as the individual data range over Q^2 , we display our predictions with selected values of Q^2 to illustrate the evolution effects. This allows us to see the comparison of data and theory in a compact, albeit approximate, manner.

5. $\alpha_s(Q^2)$ Comparisons

In our present fits, we allowed $\alpha_s(Q_0^2)$ to be a parameter of the fit; these results are summarized in Table II. We observe the variation across our different fits is minimal, and these values are consistent with the KATAO fit within uncertainties. Although these values are extracted from data in the range $1 \lesssim Q^2 \lesssim 100$, we

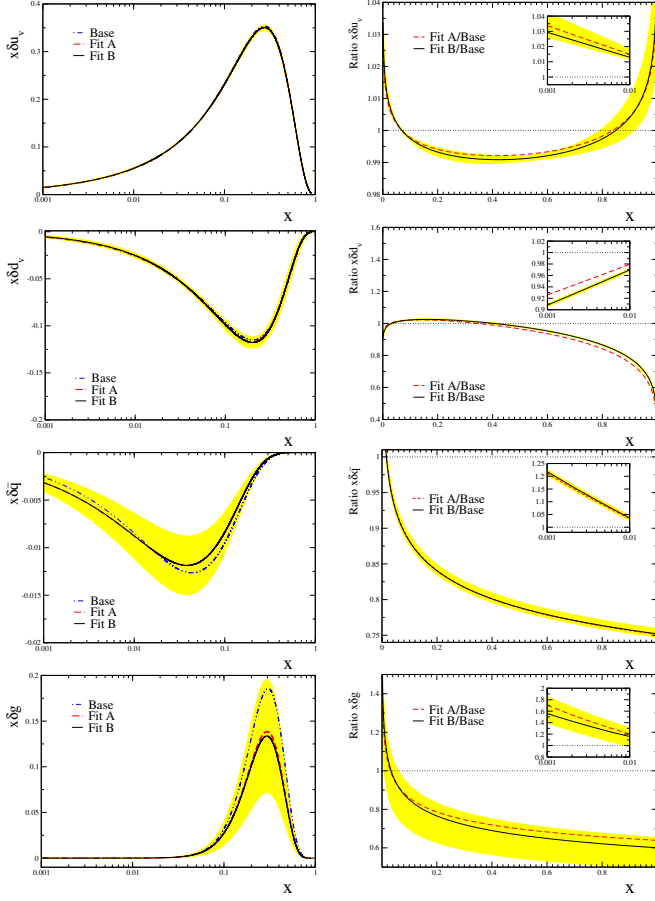


Figure 6. Left panels: polarized parton distributions at Q_0^2 as a function of x for our different cases: Base (dashed-dotted), Fit A (dashed) and Fit B (solid line) according to Table I. Only the PPDF error bands for Fit B (all data) are shown. Right panels: polarized parton distribution ratios $\delta f/\delta f_{Base}$ for Fit A (dashed) and Fit B (solid line) to Base obtained our QCD fits to the data. The impact of COMPASS data in the low x regions are shown in the inset plots.

can evolve these up to M_Z to compare with other values used in the literature. Note the $\alpha_s(Q^2)$ evolution up to the M_Z^2 scale will depend on the number of active flavors and the mass scale of the transitions; we choose $m_c^2 = 3 \text{ GeV}^2$ and $m_b^2 = 25 \text{ GeV}^2$. Extrapolating our results up to M_Z at NLO order we find $\alpha_s(M_Z^2) = 0.1161$ for Fit A and $\alpha_s(M_Z^2) = 0.1160$ for Fit B, and $\alpha_s(M_Z^2) = 0.1149$ for KATAO. These values are low but within 2σ as compared to the world average value of $\alpha_s(M_Z^2) = 0.1181 \pm 0.0011$ [93], and we display this in Fig. 9 along with various results from the literature.

C. Moments and Sum Rules

We now turn to integrated moments and sum rules. Note, the calculation of the moments integrates over the

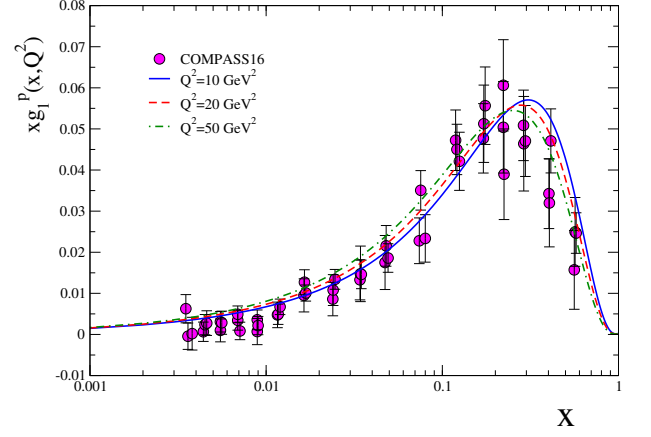


Figure 7. The COMPASS16 [65] data for the proton structure function $xg_1^p(x, Q^2)$ compared with our NLO results calculated at $Q^2 = 10, 20, 50 \text{ GeV}^2$.

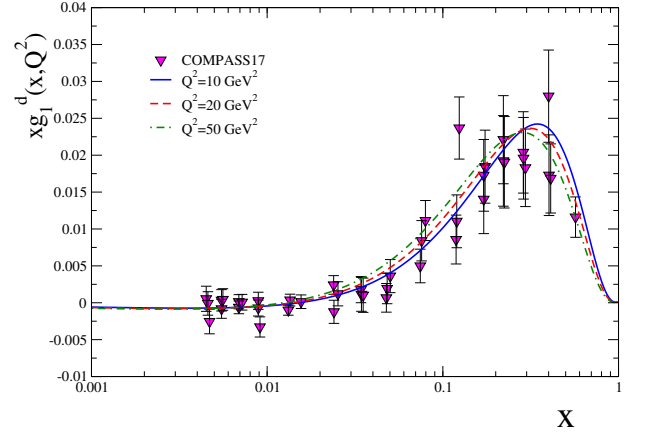


Figure 8. The COMPASS17 [66] data for the deuteron structure function $xg_1^d(x, Q^2)$ compared with our NLO results (“Fit B”) calculated at $Q^2 = 10, 20, 50 \text{ GeV}^2$.

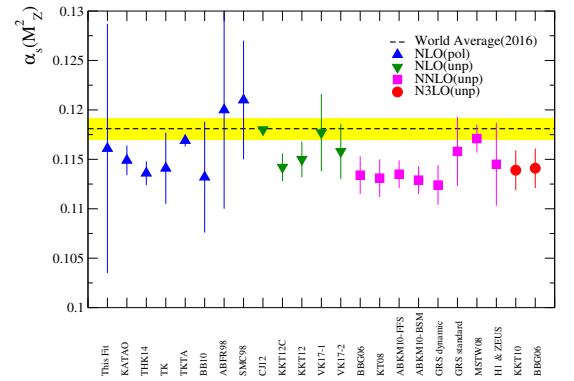


Figure 9. The strong coupling constant $\alpha_s(M_Z^2)$ values as compared with different QCD analyses at NLO [8, 20, 32, 41, 42, 45, 80–84], NNLO [85–91], and NNNLO [85, 92]. The dashed line and yellow band shows the world average $\alpha_s(M_Z^2) = 0.1181 \pm 0.0011$ [93].

full range $x = [0, 1]$, so this requires some extrapolation outside the x range where the structure functions have been measured.

1. PPDF Moments

We start by computing the PPDF moments, as these will be the necessary ingredients for the other moments and sum rules that follow.

In Table III, we compared the results of the first moments of the polarized parton densities for our fits with results from the literature at NLO in the $\overline{\text{MS}}$ -scheme at $Q^2 = 4 \text{ GeV}^2$. Comparing our “Base” fit with “Fit A” and “Fit B” we see the moments are generally stable with the exception of the Δg which varies by $\sim 30\%$. Including the other PPDF moments from the literature, we see the results for $\{\Delta u_v, \Delta d_v\}$ are quite stable ($\sim 1\%$) while $\{\Delta u, \Delta d\}$ show a bit more variation ($\sim 10\%$), and finally $\{\Delta \bar{q}, \Delta g\}$ a larger spread ($> 100\%$). We will now look at the influence of the above PPDF moments on the experimentally measurable structure functions.

2. Structure Function Moments $\Gamma_1^N(Q^2)$

We next examine the first moment of the xg_1^N ($N = p, d, n$) structure functions defined to be:

$$\Gamma_1^N(Q^2) \equiv \int_0^1 g_1^N(x, Q^2) dx. \quad (17)$$

In Table IV, we compare the results for $\Gamma_1^N(Q^2)$ of Fit B with the COMPASS measurements. We observe the fit agrees with the COMPASS results within $\sim 1\sigma$ of the experimental uncertainty.

Next, in Table V, we compare our first moment results with those from the literature. The theoretical results for Γ_1^p are uniform within $\pm 2\%$, while the range on Γ_1^d increases to $\pm 5\%$, and the range on Γ_1^n further increases to $\pm 15\%$.

3. Bjorken Sum Rule, $xg_1^{NS}(x, Q^2)$ and $\Gamma_1^{NS}(Q^2)$

Having computed the above $\Gamma_1^N(Q^2)$ moments, we can then consider the non-singlet moment $\Gamma_1^{NS}(Q^2)$ which enters the polarized Bjorken sum rule [94]

$$\begin{aligned} \Gamma_1^{NS}(Q^2) &= \int_0^1 g_1^{NS}(x, Q^2) dx \\ &= \frac{1}{6} \left| \frac{g_A}{g_V} \right| C_1^{NS}(Q^2). \end{aligned} \quad (18)$$

$\Gamma_1^{NS}(Q^2)$ is related to the ratio of the axial and vector coupling constants ($g_{A,V}$). Here, $C_1^{NS}(Q^2)$ is the non-singlet coefficient function.

The $g_1^{NS}(x, Q^2)$ can be related to the proton and neutron structure functions as [48]

$$\begin{aligned} xg_1^{NS}(x, Q^2) &\equiv xg_1^p(x, Q^2) - xg_1^n(x, Q^2) \\ &= 2[xg_1^p(x, Q^2) - \frac{xg_1^d(x, Q^2)}{1 - \frac{3}{2}\omega_D}]. \end{aligned} \quad (19)$$

In Fig. 10 we compare our results for $xg_1^{NS}(x, Q^2)$ with the HERMES experimental data [48] for selected bins of Q^2 . We find minimal variation among our different theoretical fits (including the previous KATAO fit), and these curves compare well with the experimental results.

From Eq. 19 we can also relate $\Gamma_1^{NS}(Q^2)$ to the previously computed proton and neutron first moments as:

$$\Gamma_1^{NS}(Q^2) = \Gamma_1^p(Q^2) - \Gamma_1^n(Q^2) \quad .$$

These results are presented in Table V and with the COMPASS results. The result of our “Fit B” is comparable to COMPASS16, and below (but within uncertainties) to COMPASS17.

4. $g_2^N(x, Q^2)$ Structure Functions

We can also calculate the structure function $g_2^N(x, Q^2)$ via the Wandzura-Wilczek relation [98, 99]:

$$g_2^N(x, Q^2) = -g_1^N(x, Q^2) + \int_x^1 \frac{dy}{y} g_1^N(y, Q^2). \quad (20)$$

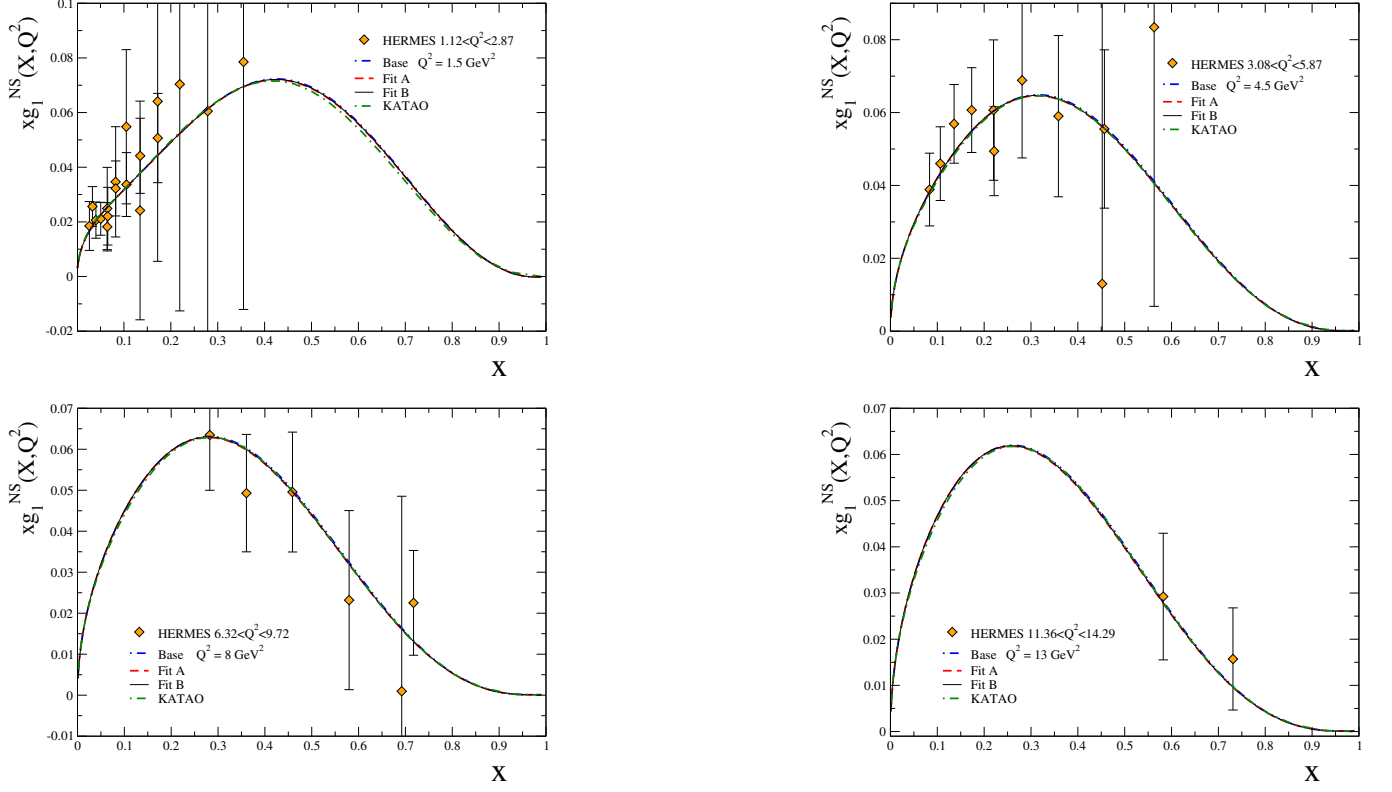
Figure 11 shows the polarized structure function xg_2^p and xg_2^d as a function of x for different cases of Base, Fit A, Fit B and our previous KATAO results [41] in comparison with E143 [54], E155 [95], HERMES [96], SMC [97], E143 [54] and E155 [95] experimental data at $Q^2 = 5, 6 \text{ GeV}^2$. As the data actually span over a range of Q^2 , in Figure 12 we display the Q^2 evolution of the polarized structure function $xg_2(x, Q^2)$ for the proton and deuteron as function of x . In Figure 11 we see that our “Base” and “Fit A” coincide throughout the x range suggesting a minimal impact from the COMPASS16 data on this observable; conversely, our “Fit B” does differ, especially in the larger x region, suggesting a stronger influence of the COMPASS17 data on $xg_2^d(x, Q^2)$.

D. The Proton Spin

It is important for us to understand the decomposition of the proton spin in terms of the separate contributions from the quarks, gluon, and the orbital angular momentum components. The spin of the proton can be

Table III. Comparison of the first moments of the polarized parton densities at NLO in the $\overline{\text{MS}}$ -scheme at $Q^2 = 4 \text{ GeV}^2$.

	Base	Fit A	Fit B	KATAO [41]	BB [32]	GRSV [21]	AAC [25]
Δu_v	0.928	0.928	0.928	0.928	0.928	0.9206	0.9278
Δd_v	-0.342	-0.342	-0.342	-0.342	-0.342	-0.3409	-0.3416
Δu	0.881	0.880	0.880	0.874	0.866	0.8593	0.8399
Δd	-0.389	-0.390	-0.390	-0.396	-0.404	-0.4043	-0.4295
$\Delta \bar{q}$	-0.047	-0.048	-0.048	-0.054	-0.066	-0.0625	-0.0879
Δg	0.218	0.167	0.162	0.224	0.462	0.6828	0.8076

Figure 10. NLO non-singlet polarized structure function $xg_1^{NS}(x, Q^2)$ as function of x in comparison with the results of KATAO [41] and HERMES experimental data [48].Table IV. First moments of the polarized structure function $\{\Gamma_1^p, \Gamma_1^d, \Gamma_1^n, \Gamma_1^{NS}\}$ for “Fit B” at $Q^2 = 3 \text{ GeV}^2$ compared with COMPASS16 [65] and COMPASS17 [66] experimental data.

	Fit B	COMPASS16 [65]	COMPASS17 [66]
Γ_1^p	0.134	$0.139 \pm 0.003 \pm 0.009$	-
Γ_1^d	0.041	-	$0.043 \pm 0.001 \pm 0.003$
Γ_1^n	-0.045	$-0.041 \pm 0.006 \pm 0.011$	-
Γ_1^{NS}	0.179	$0.181 \pm 0.008 \pm 0.014$	$0.192 \pm 0.007 \pm 0.015$

computed from the first moment of the polarized parton densities together with the quark and gluon orbital momentum (L_q, L_g) is as following [100]

$$\frac{1}{2} = \frac{1}{2} \Delta \Sigma(Q^2) + \Delta g(Q^2) + L_z(Q^2). \quad (21)$$

Table V. First moments of the polarized structure functions $\{\Gamma_1^p, \Gamma_1^d, \Gamma_1^n\}$ at $Q^2 = 5 \text{ GeV}^2$ for “Fit B” as compared to other results from the literature at NLO in the $\overline{\text{MS}}$ -scheme.

	Fit B	KATAO [41]	GRSV [21]	AAC [25]
Γ_1^p	0.136	0.133	0.132	0.137
Γ_1^d	0.041	0.036	0.032	0.038
Γ_1^n	-0.047	-0.053	-0.062	-0.056

Here $L_z(Q^2) = L_q(Q^2) + L_g(Q^2)$ is the total orbital angular momentum of all the quarks and gluons, $\Delta g(Q^2) = \int_0^1 dx \delta g(x, Q^2)$ is the first moment of the polarized gluon distribution, and $\Delta \Sigma(Q^2) = \int_0^1 dx \delta \Sigma(x, Q^2)$ with $\delta \Sigma \equiv \delta u_v + \delta d_v + 6\delta \bar{q}$ is the first moment of the polarized singlet distribution. In Eq. (21), we note that the spin

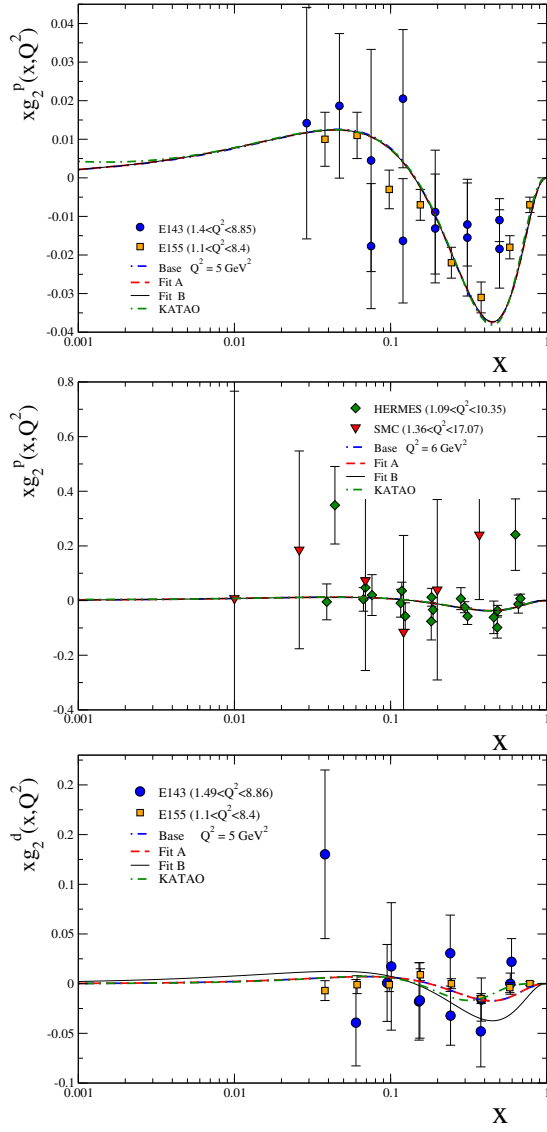


Figure 11. NLO polarized structure function $xg_2^p(x, Q^2)$ and $xg_2^d(x, Q^2)$ as a function of x for $Q^2 = 5, 6 \text{ GeV}^2$ compared to E143 [54], E155 [95], HERMES [96], SMC [97] experimental data. We present also the results of different Base (dashed-dotted-dotted), Fit A (dashed) and Fit B (solid line) QCD fits which are compared with our previous KATAO (dashed-dotted) results.

Table VI. Spin contribution of the proton in the NLO approximations at $Q^2 = 4 \text{ GeV}^2$ for Base, Fit A, Fit B compared with the KATAO [41]. We have computed $\{\frac{1}{2}\Delta\Sigma, \Delta g\}$ using our PDFs, and inferred L_z assuming precisely $1/2$ for the proton spin.

	$\frac{1}{2}\Delta\Sigma$	Δg	L_z	$\frac{1}{2}\Delta\Sigma + \Delta g + L_z$
KATAO	0.131	0.224	0.145	$1/2$
Base	0.152	0.218	0.130	$1/2$
Fit A	0.149	0.167	0.184	$1/2$
Fit B	0.149	0.162	0.189	$1/2$

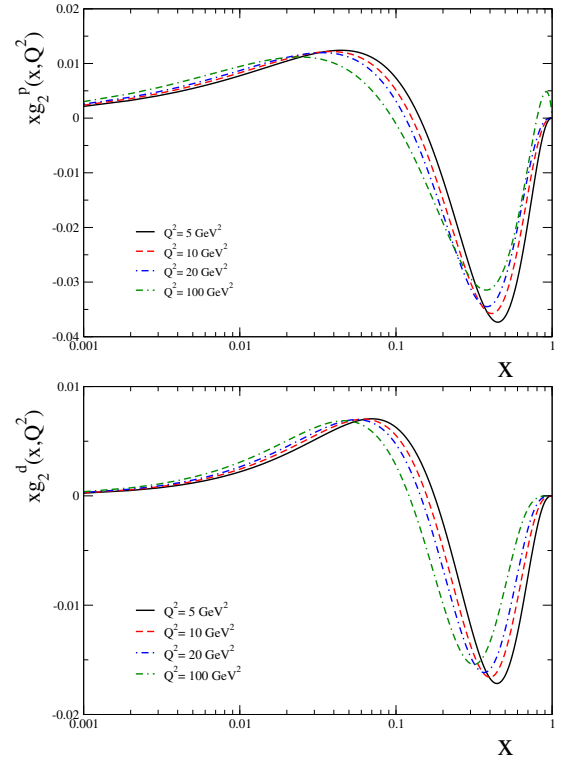


Figure 12. NLO polarized structure function $xg_2(x, Q^2)$ for the proton and deuteron as function of x and for $Q^2 = 5, 10, 20, 100 \text{ GeV}^2$.

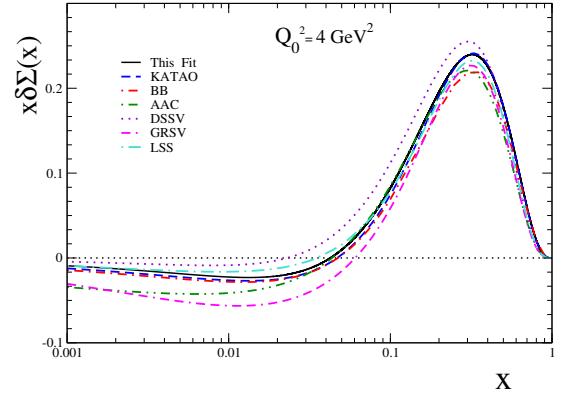


Figure 13. NLO polarized singlet parton density $x\delta\Sigma(x)$ at $Q_0^2 = 4 \text{ GeV}^2$ for this fit ("Fig B") as a function of x , compared with results from the literature including KATAO [41], BB [32], AAC [25], DSSV [30], GRSV [21] and LSS [34].

sum ($1/2$) is actually independent of Q^2 even though each individual term is dependent on Q^2 .

In Table VI we compute $\{\frac{1}{2}\Delta\Sigma, \Delta g\}$ using "Fit B" at $Q^2 = 4 \text{ GeV}^2$, and then infer the value of $L_z(Q^2)$ assuming Eq. (21). As we observed in Table III the values for $\frac{1}{2}\Delta\Sigma$ show minimal variation while there is a larger spread for $\Delta g(Q^2)$ which then implies a larger spread of L_z .

The comparison of "Fit B" with other $x\delta g(Q^2)$ from

the literature were displayed in Figure 5, and there is quite a bit of variation. In contrast, Figure 13 shows our NLO singlet polarized parton density $x\delta\Sigma(x)$ ($\equiv \delta u_v + \delta d_v + 6\delta\bar{q}$) compared with other results from the literature. The results of this fit (“Fit B”) with the previous analysis KATAO [41] are quite similar as suggested by Table III. Generally, the singlet polarized distributions are negative for $x \lesssim 0.04$ for most of the models, but there is some slight variation in the range $x \lesssim 0.06$ to $x \lesssim 0.02$. Overall, the variation of $x\delta\Sigma(x)$, as compared to $x\delta g(Q^2)$, is reduced; this is notable as $x\delta\Sigma(x)$ is a combination of both valence and sea PPDFs.

V. CONCLUSIONS

We performed a QCD analysis of the deep inelastic nucleon scattering data from COMPASS [60–62], HERMES [48–50], SLAC [51, 53–57], EMC [58], and SMC [59] at NLO. This also included the recent data from COMPASS16 [65] and COMPASS17 [66] for the proton and deuteron polarized structure function measurements.

We extracted the PPDFs and $\alpha_s(Q_0^2)$ with uncertainties using a χ^2 minimization, and compared our results with those from the literature including AAC [25], BB [32], GRSV [21], LSS [34] and KATAO [41]. In contrast to our previous polarized analysis (KATAO), we did not use the Jacobi polynomial expansion method. Our results for the PPDFs are comparable to other extractions, and generally it appears that $x\delta u_v$ and $x\delta d_v$ are comparatively well determined in contrast to $x\delta\bar{q}$ and $x\delta g$ which display a larger variation across the x range.

We also computed various structure functions and moments for the proton, neutron, and deuteron, and these also compare well with the both the COMPASS data, as

well as other determinations from the literature. Again the results from this fit are comparable to the previous KATAO [41] results using orthogonal polynomials; this is reassuring to see the results are generally independent of the underlying calculational methodology.

The strong coupling constant $\alpha_s(Q_0^2)$ was extracted from the fits, and the uncertainty is slightly decreased compared to the KATAO analysis. This $\alpha_s(Q_0^2)$ can be evolved up to $\alpha_s(M_Z^2)$ by assuming an evolution order (LO, NLO, ...) and heavy quark mass thresholds; we find values that are low compared to the world average, but within uncertainties.

From this analysis, it appears that both the various theoretical analyses using a variety of techniques and (x -space, N -space, orthogonal polynomials) are generally converging to yield a homogeneous set of predictions which are in good agreement with the diverse sets of experimental measurements. While there is still room for further improvements, such studies provide a strong validation of the underlying QCD theoretical framework.

A standard LHAPDF library file of our polarized PDFs $\{x\delta u_v(x, Q^2), x\delta d_v(x, Q^2), x\delta\bar{q}(x, Q^2), x\delta g(x, Q^2)\}$ and their uncertainties can be obtained via e-mail from the authors upon request.

ACKNOWLEDGMENTS

We gratefully acknowledge O. Denisov and E. Kabuss of the COMPASS collaboration for detailed comments and helpful discussions. We also thank F. Arbabifar and M. Soleymanini for useful comments. A. K. is grateful to CERN TH-PH division for the hospitality where a portion of this work was performed. The work of F.O. was supported in part by the U.S. Department of Energy under Grant No. DE-SC0010129.

-
- [1] S. D. Bass, Rev. Mod. Phys. **77**, 1257 (2005), hep-ph/0411005. I
 - [2] S. E. Kuhn, J. P. Chen, and E. Leader, Prog. Part. Nucl. Phys. **63**, 1 (2009), 0812.3535. I
 - [3] M. Anselmino, A. Efremov, and E. Leader, Phys. Rept. **261**, 1 (1995), [Erratum: Phys. Rept.281,399(1997)], hep-ph/9501369. I
 - [4] B. Lampe and E. Reya, Phys. Rept. **332**, 1 (2000), hep-ph/9810270. II
 - [5] E. W. Hughes and R. Voss, Ann. Rev. Nucl. Part. Sci. **49**, 303 (1999).
 - [6] B. W. Filippone and X.-D. Ji, Adv. Nucl. Phys. **26**, 1 (2001), hep-ph/0101224.
 - [7] G. Altarelli (2009), hep-ph/0907.1751. I
 - [8] G. Altarelli, R. D. Ball, S. Forte, and G. Ridolfi, Acta Phys. Polon. **B29**, 1145 (1998), hep-ph/9803237. I, 9
 - [9] R. D. Ball, G. Ridolfi, G. Altarelli, and S. Forte, AIP Conf. Proc. **407**, 834 (1997), hep-ph/9707276.
 - [10] C. Bourrely, F. Buccella, O. Pisanti, P. Santorelli, and J. Soffer, Prog. Theor. Phys. **99**, 1017 (1998), hep-ph/9803229.
 - [11] D. de Florian, O. A. Sampayo, and R. Sassot, Phys. Rev. **D57**, 5803 (1998), hep-ph/9711440.
 - [12] D. de Florian and R. Sassot, Phys. Rev. **D62**, 094025 (2000), hep-ph/0007068.
 - [13] D. de Florian, G. A. Navarro, and R. Sassot, Phys. Rev. **D71**, 094018 (2005), hep-ph/0504155.
 - [14] L. E. Gordon, M. Goshtasbpour, and G. P. Ramsey, Phys. Rev. **D58**, 094017 (1998), hep-ph/9803351.
 - [15] E. Leader, A. V. Sidorov, and D. B. Stamenov, Phys. Lett. **B462**, 189 (1999), hep-ph/9905512.
 - [16] E. Leader, A. V. Sidorov, and D. B. Stamenov, Phys. Lett. **B445**, 232 (1998), hep-ph/9808248.
 - [17] E. Leader, A. V. Sidorov, and D. B. Stamenov, Phys. Rev. **D58**, 114028 (1998), hep-ph/9807251.
 - [18] E. Leader, A. V. Sidorov, and D. B. Stamenov, Int. J. Mod. Phys. **A13**, 5573 (1998), hep-ph/9708335.
 - [19] M. Stratmann, Nucl. Phys. Proc. Suppl. **79**, 538 (1999), hep-ph/9907465.

- [20] D. K. Ghosh, S. Gupta, and D. Indumathi, Phys. Rev. **D62**, 094012 (2000), hep-ph/0001287. 9
- [21] M. Gluck, E. Reya, M. Stratmann, and W. Vogelsang, Phys. Rev. **D63**, 094005 (2001), hep-ph/0011215. IV B 2, 5, III, V, 13, V
- [22] R. S. Bhallerao, Phys. Rev. **C63**, 025208 (2001), hep-ph/0003075.
- [23] E. Leader, A. V. Sidorov, and D. B. Stamenov, Eur. Phys. J. **C23**, 479 (2002), hep-ph/0111267.
- [24] J. Blumlein and H. Bottcher, Nucl. Phys. **B636**, 225 (2002), hep-ph/0203155. II
- [25] Y. Goto et al. (Asymmetry Analysis), Phys. Rev. **D62**, 034017 (2000), hep-ph/0001046. III A, IV B 2, 5, III, V, 13, V
- [26] E. Leader, A. V. Sidorov, and D. B. Stamenov, Phys. Rev. **D73**, 034023 (2006), hep-ph/0512114.
- [27] C. Bourrely, J. Soffer, and F. Buccella, Eur. Phys. J. **C23**, 487 (2002), hep-ph/0109160.
- [28] S. Forte, M. L. Mangano, and G. Ridolfi, Nucl. Phys. **B602**, 585 (2001), hep-ph/0101192.
- [29] G. Altarelli, R. D. Ball, S. Forte, and G. Ridolfi, Nucl. Phys. **B496**, 337 (1997), hep-ph/9701289.
- [30] D. de Florian, R. Sassot, M. Stratmann, and W. Vogelsang, Phys. Rev. Lett. **101**, 072001 (2008), 0804.0422. IV B 2, 5, 13
- [31] M. Hirai and S. Kumano (Asymmetry Analysis), Nucl. Phys. **B813**, 106 (2009), 0808.0413.
- [32] J. Blumlein and H. Bottcher, Nucl. Phys. **B841**, 205 (2010), 1005.3113. II, IV B 2, 5, 9, III, 13, V
- [33] D. de Florian, R. Sassot, M. Stratmann, and W. Vogelsang, Phys. Rev. **D80**, 034030 (2009), 0904.3821.
- [34] E. Leader, A. V. Sidorov, and D. B. Stamenov, Phys. Rev. **D82**, 114018 (2010), 1010.0574. IV B 2, 5, 13, V
- [35] E. Leader, A. V. Sidorov, and D. B. Stamenov, Phys. Rev. **D84**, 014002 (2011), 1103.5979.
- [36] E. Leader, A. V. Sidorov, and D. B. Stamenov (2010), 1007.4781.
- [37] E. Leader, A. V. Sidorov, and D. B. Stamenov, Phys. Rev. **D80**, 054026 (2009), 0908.2390.
- [38] E. Leader, A. V. Sidorov, and D. B. Stamenov, Phys. Rev. **D75**, 074027 (2007), hep-ph/0612360.
- [39] R. D. Ball, S. Forte, A. Guffanti, E. R. Nocera, G. Ridolfi, and J. Rojo (NNPDF), Nucl. Phys. **B874**, 36 (2013), 1303.7236.
- [40] E. R. Nocera, Phys. Lett. **B742**, 117 (2015), 1410.7290. I
- [41] A. N. Khorramian, S. Atashbar Tehrani, S. Taheri Monfared, F. Arbabifar, and F. I. Olness, Phys. Rev. **D83**, 054017 (2011), 1011.4873. I, III, II, IV B 2, IV B 2, 5, 9, IV C 4, III, 10, V, VI, 13, IV D, V
- [42] S. Atashbar Tehrani and A. N. Khorramian, JHEP **07**, 048 (2007), 0705.2647. 9
- [43] A. N. Khorramian, A. Mirjalili, and S. A. Tehrani, JHEP **10**, 062 (2004), hep-ph/0411390. I
- [44] S. Atashbar Tehrani, F. Taghavi-Shahri, A. Mirjalili, and M. M. Yazdanpanah, Phys. Rev. **D87**, 114012 (2013), [Erratum: Phys. Rev. **D88**, no.3, 039902(2013)]. I
- [45] F. Taghavi-Shahri, H. Khanpour, S. Atashbar Tehrani, and Z. Alizadeh Yazdi, Phys. Rev. **D93**, 114024 (2016), 1603.03157. 9
- [46] H. Khanpour, S. T. Monfared, and S. Atashbar Tehrani, Phys. Rev. **D96**, 074037 (2017), 1710.05747.
- [47] H. Khanpour, S. T. Monfared, and S. Atashbar Tehrani, Phys. Rev. **D95**, 074006 (2017), 1703.09209. I
- [48] A. Airapetian et al. (HERMES), Phys. Rev. **D75**, 012007 (2007), hep-ex/0609039. I, III, III B, III B, III B, 2, 3, 4, IV C 3, IV C 3, 10, V
- [49] K. Ackerstaff et al. (HERMES), Phys. Lett. **B404**, 383 (1997), hep-ex/9703005. III, 2, 4
- [50] A. Airapetian et al. (HERMES), Phys. Lett. **B442**, 484 (1998), hep-ex/9807015. I, III, III B, III B, 2, 4, V
- [51] P. L. Anthony et al. (E142), Phys. Rev. **D54**, 6620 (1996), hep-ex/9610007. I, III, III B, 4, V
- [52] K. Abe et al. (E154), Phys. Lett. **B405**, 180 (1997), hep-ph/9705344.
- [53] K. Abe et al. (E154), Phys. Rev. Lett. **79**, 26 (1997), hep-ex/9705012. III, III B, 4, V
- [54] K. Abe et al. (E143), Phys. Rev. **D58**, 112003 (1998), hep-ph/9802357. III, III B, III B, 2, 3, IV C 4, IV C 4, 11
- [55] P. L. Anthony et al. (E155), Phys. Lett. **B463**, 339 (1999), hep-ex/9904002. III, III B, 3
- [56] J. Ashman et al. (European Muon), Nucl. Phys. **B328**, 1 (1989). III, III B, 3
- [57] P. L. Anthony et al. (E155), Phys. Lett. **B493**, 19 (2000), hep-ph/0007248. I, III, III B, 2, V
- [58] J. Ashman et al. (European Muon), Phys. Lett. **B206**, 364 (1988). I, III, III B, 2, V
- [59] B. Adeva et al. (Spin Muon), Phys. Rev. **D58**, 112001 (1998). III, III B, III B, 2, 3, V
- [60] M. G. Alekseev et al. (COMPASS), Phys. Lett. **B690**, 466 (2010), 1001.4654. III, III B, 2, V
- [61] E. S. Ageev et al. (COMPASS), Phys. Lett. **B612**, 154 (2005), hep-ex/0501073. III, III B, 3
- [62] V. Yu. Alexakhin et al. (COMPASS), Phys. Lett. **B647**, 8 (2007), hep-ex/0609038. I, III, III B, 3, V
- [63] K. V. Dharmawardane et al. (CLAS), Phys. Lett. **B641**, 11 (2006), nucl-ex/0605028. I
- [64] X. Zheng et al. (Jefferson Lab Hall A), Phys. Rev. **C70**, 065207 (2004), nucl-ex/0405006. I
- [65] C. Adolph et al. (COMPASS), Phys. Lett. **B753**, 18 (2016), 1503.08935. I, III, III, III B, III B, 2, IV, IV A 1, IV B 4, 7, IV, V
- [66] C. Adolph et al. (COMPASS), Phys. Lett. **B769**, 34 (2017), 1612.00620. I, III, III, III B, III B, IV, 3, IV A 1, IV B 4, 8, IV, V
- [67] W. Vogelsang, Phys. Rev. **D54**, 2023 (1996), hep-ph/9512218. II
- [68] W. Furmanski and R. Petronzio, Z. Phys. **C11**, 293 (1982). II
- [69] G. T. Bodwin and J.-W. Qiu, Phys. Rev. **D41**, 2755 (1990). II
- [70] E. B. Zijlstra and W. L. van Neerven, Nucl. Phys. **B417**, 61 (1994), [Erratum: Nucl. Phys. **B501**, 599(1997)]. II
- [71] A. Vogt, Comput. Phys. Commun. **170**, 65 (2005), hep-ph/0408244. II, II
- [72] M. Lacombe, B. Loiseau, R. Vinh Mau, J. Cote, P. Pires, and R. de Tourreil, Phys. Lett. **101B**, 139 (1981). II
- [73] M. A. Ahmed and G. G. Ross, Nucl. Phys. **B111**, 441 (1976). II
- [74] R. Mertig and W. L. van Neerven, Z. Phys. **C70**, 637 (1996), hep-ph/9506451. II
- [75] M. Gluck, E. Reya, and A. Vogt, Z. Phys. **C48**, 471 (1990). II
- [76] J. Blumlein and A. Vogt, Phys. Rev. **D58**, 014020 (1998), hep-ph/9712546. II
- [77] F. Arbabifar, A. N. Khorramian, and M. Soleymaninia, Phys. Rev. **D89**, 034006 (2014), 1311.1830. II, II, 1,

III A

- [78] C. Amsler et al. (Particle Data Group), Phys. Lett. **B667**, 1 (2008). III A
- [79] F. James (1994). III B
- [80] S. Taheri Monfared, Z. Haddadi, and A. N. Khorramian, Phys. Rev. **D89**, 074052 (2014), [Erratum: Phys. Rev.D89,no.11,119901(2014)], 1405.4633. 9
- [81] H. Khanpour, A. N. Khorramian, and S. A. Tehrani, J. Phys. **G40**, 045002 (2013), 1205.5194.
- [82] B. Adeva et al. (Spin Muon), Phys. Rev. **D58**, 112002 (1998).
- [83] A. Vafae and A. N. Khorramian, Nucl. Phys. **B921**, 472 (2017), 1709.08346.
- [84] A. Vafae and A. Khorramian, Eur. Phys. J. **A53**, 220 (2017), 1711.06573. 9
- [85] J. Blumlein, H. Bottcher, and A. Guffanti, Nucl. Phys. **B774**, 182 (2007), hep-ph/0607200. 9
- [86] A. N. Khorramian and S. A. Tehrani, Phys. Rev. **D78**, 074019 (2008), 0805.3063.
- [87] S. Alekhin, J. Blumlein, S. Klein, and S. Moch, Phys. Rev. **D81**, 014032 (2010), 0908.2766.
- [88] M. Gluck, E. Reya, and C. Schuck, Nucl. Phys. **B754**, 178 (2006), hep-ph/0604116.
- [89] A. D. Martin, W. J. Stirling, R. S. Thorne, and G. Watt, Eur. Phys. J. **C64**, 653 (2009), 0905.3531.
- [90] F. D. Aaron et al. (ZEUS, H1), JHEP **01**, 109 (2010), 0911.0884.
- [91] D. d’Enterria, ed., *Proceedings, High-Precision α_s Measurements from LHC to FCC-ee*, CERN (CERN, Geneva, 2015), 1512.05194, URL <https://inspirehep.net/record/1409920/files/arXiv:1512.05194.pdf>. 9
- [92] A. N. Khorramian, H. Khanpour, and S. A. Tehrani, Phys. Rev. **D81**, 014013 (2010), 0909.2665. 9
- [93] C. Patrignani et al. (Particle Data Group), Chin. Phys. **C40**, 100001 (2016). IV B 5, 9
- [94] J. D. Bjorken, Phys. Rev. **D1**, 1376 (1970). IV C 3
- [95] P. L. Anthony et al. (E155), Phys. Lett. **B553**, 18 (2003), hep-ex/0204028. IV C 4, IV C 4, 11
- [96] A. Airapetian et al. (HERMES), Eur. Phys. J. **C72**, 1921 (2012), 1112.5584. IV C 4, 11
- [97] D. Adams et al. (Spin Muon (SMC)), Phys. Rev. **D56**, 5330 (1997), hep-ex/9702005. IV C 4, 11
- [98] S. Wandzura and F. Wilczek, Phys. Lett. **72B**, 195 (1977). IV C 4
- [99] A. Piccione and G. Ridolfi, Nucl. Phys. **B513**, 301 (1998), hep-ph/9707478. IV C 4
- [100] E. Leader (2016), 1604.00305. IV D